Supporting Information

BCC-Phased PdCu Alloy as a Highly Active Electrocatalyst for Hydrogen Oxidation in Alkaline Electrolytes

Yang Qiu,[†‡] Le Xin,[†‡] Yawei Li,[§‡] Ian T. McCrum,[§] Fangmin Guo,[∥] Tao Ma,[⊥] Yang Ren,[∥] Qi Liu,[∥] Lin Zhou,[⊥] Shuang Gu,[#] Michael J. Janik,[§] and Wenzhen Li[*, †⊥]

† Department of Chemical and Biological Engineering, Iowa State University, 618 Bissell Rd, Ames, Iowa, 50011, United Sates

§ Department of Chemical Engineering, Pennsylvania State University, 51 Greenberg Building, University Park, Pennsylvania, 16802, United States

∥ Advanced Photon Source, Argonne National Laboratory, 9700 South Cass Avenue, Argonne, Illinois 60439, United States

⊥ Ames Laboratory, U.S. Department of Energy, 311 Iowa State University, Ames, Iowa 50011, United States

 # Department of Mechanical Engineering, Wichita State University, 1845 Fairmount St. Wichita, Kansas, 67260, United States

Email: Wenzhen Li wzli@iastate.edu

Table of Contents **Page**

Number of figures = 11, Number of tables = 4.

I. Materials Synthesis and Physical Characterization

Materials

$Pd(acac)_2$ (99%, Sigma Aldrich), $Cu(acac)_2$ (≥99.9%, Sigma Aldrich), Oleylamine (70%, Sigma Aldrich), Ascorbic acid (≥99%, Sigma Aldrich), Oleic acid (≥99%, Sigma Aldrich), benzyl ether (98%, Sigma Aldrich), $LiBEt_3H$ (1.0 M lithium triethylborohydride in THF), 5 wt% Nafion solution (in iso-propanol, Ion Power), KOH (≥85%, Sigma Aldrich), Acetic acid (99.7% w/w, Fisher scientific) were purchased and used without further purification for all experiments. Vulcan XC-72R carbon black (Fuel Cell store) as catalysts supporting materials were pre-treated at 120°C in Air and stored in vacuum oven at 80°C. UHP N_2 (99.999%, Airgas), UHP H_2 (99.999%, Airgas), and UHP CO (99.999%, Matheson) were used for electrochemical property characterizations.

Synthesis of PdCu/C-raw, Pd/C catalysts

The PdCu/C (Pd:Cu atomic ratio = 1:1) samples were prepared through one-step wet-chemical method which has been widely used for nano-particle synthesis previously.[5] Typically, 68.0 mg of Vulcan XC-72R carbon black was dispersed in 40 ml of benzyl ether at room temperature, followed by ultra-sonication for 30min to obtain uniform mixture. The 0.1 mmol of $Pd(acac)_2$ and 0.1 mmol of $Cu(acac)_2$ were then dissolved into mixture with stirring. After 30 min UHP N_2 purging, the mixture was heated to 100 °C, followed by adding 400 μL of oleylamine and 200 μL of oleic acid adding and holding for 10min to get uniform solution. As the temperature was increased to 150 °C, 1.0 mL of $LiBEt_3H$ solution was quickly injected into the system. The temperature was held for 10 min, and then quickly increased to 210 °C. After holding for an additional 45 min, the final products were collected by filtration, washed with copious ethanol, and dried in vacuum oven at 60 °C overnight. A control sample, Pd/C, was synthesized via a similar method discussed above, except $Cu(acac)_2$ metal salt introduction. The metal loading of as-synthesized PdCu/C-raw and Pd/C samples were determined to be ~20 wt%.

Synthesis of PdCu/C-T (200 °C to 600 °C)

A 30 mg PdCu/C-raw sample was subjected to thermal annealing with different temperature from 200 °C to 600 °C with 10 °C/min heating rate under 100 ml/min UHP N_2 purging condition for 4 h. The obtained PdCu/C-T (T=200 °C to 600 °C) materials were finally stored in 20 ml-type glass vial.

Synthesis of BCC PdCu/C-400°C*

Typically, 0.1 mmol of $Pd(acac)_2$, 0.2 mmol of $Cu(acac)_2$, and 142.4 mg of ascorbic acid were dissolved into 20 ml oleylamine with stirring. After UHP N_2 purging for 30 min, the solution was heated to 60 °C to fully dissolve ascorbic acid. The temperature was quickly increased to 200 °C and held for 5 h with stirring. The solution becomes dark color at around 80 °C. The PdCu NPs were collected by centrifugation and washed by acetone / ethanol mixture several times, and dried in vacuum oven at 60 °C overnight. The obtained PdCu NPs were dispersed in hexane, followed by drop casting in Vulcan XC-72R carbon

black & hexane mixture. The PdCu/C was collected by centrifugation and washed by copious ethanol. The final products were dried in vacuum oven at 60 °C overnight. The metal loading was determined to be ~20 wt%.

The as-prepared PdCu/C powders were subjected to thermal annealing at 400 °C with 10 °C/min heating rate under 100 ml/min UHP N_2 purging condition for 4 h. The obtained BCC PdCu/C-400°C* sample was washed by diluted acetic acid, followed by the drying in vacuum oven at 60 °C overnight. The final products were stored in 20 ml-type glass vial.

Physical characterization

The Inductively coupled plasma-optical emission spectroscopy (ICP-OES, Perkin Elmer Optima 8000 instrument) was utilized to determine the Pd/Cu weight and atomic ratio of as-synthesized PdCu/C catalysts. 10 to 15 mg PdCu/C powders were dispersed into concentrated aqua regia with stirring for Pd and Cu dissolving, followed by the dilution with DI H_2O and filtering to obtain PdCu dissolved 4% aqua regia sample solution. Thermogravimetric (TGA, Discovery series) and simultaneous modules were employed to measure the mass loss of PdCu/C catalysts in UHP N_2 has with heating rate of 5 °C/min from 30 °C to 620 °C.

The ex-situ XRD patterns were obtained from a Rigaku Ultima IV X-ray diffraction (XRD) systems (1D acquisition mode) with Cu Kα radiation (λ = 1.5406 Å) at room temperature, with a tube current of 30 mA and a tube voltage of 40 kV. The in-situ XRD patterns were achieved at Argonne National lab 11-ID-C beam line with high energy radiation (λ = 0.774902 Å). The sample was heated from 200 °C to 900 °C with 2 °C/min rate, and held 15 s per 2 °C for sample scanning.

JEOL 2100 200 kV scanning and transmission electron microscope (STEM) was utilized to determine the PdCu NPs dispersion, particle size, and size distribution of as-synthesized PdCu/C catlaysts. High-angle annular dark-field STEM (HAADF-STEM) imaging, element mapping, and line scanning was performed on Titan Themis 300 probe corrected TEM with a Super-X EDX detector from Sensitive Instrument Facility of Ames lab. To avoid the sample grid interference, the TEM sample of PdCu/C catalysts were prepared by using Au TEM grid. X-ray photoelectron spectroscopy (XPS) with Mg K alpha X-ray (1253.6 eV) (Kratos Amicus/ESCA 3400) was used to determine the Pd/Cu concentrations and their corresponding chemical/valence status through different binding energy peaks.

II. Electrochemical characterization

Electrode preparation

All electrocatalytic property characterizations were conducted in a three-electrode system using electrochemical potentiostat (VSP-300, Bio-Logic). A coiled Pt-wire, which is isolated by a fritted glass tube from the main test electrolyte, and a 0.1 M KOH filled Hg/HgO electrode were utilized as counter and reference electrode in the three-electrode

system, respectively. To fabricate the working electrode, a 1.0 mg/ml of catalyst ink was prepared by adding PdCu/C powders in iso-propanol (IPA), followed by 30 min of ultra-sonication so as to fully disperse particles in the solvent. 20 µl of catalyst ink was drop-casted onto the glassy carbon electrode surface with a Pd loading of ~12.5 $\mu g_{Pd}/cm^2_{geo}$, and 10 µl of IPA diluted 0.05 wt% Nafion solution was finally dropped on the surface of PdCu/C. After 30 min air drying at ambient temperature, a uniform catalyst thin-film was obtained for following electrochemical measurements. The Pt/C, Pd/C and Cu/C RDE electrode were also fabricated with a Pt or Cu loading of ~12.5 $\mu g_{metal}/cm^2_{geo}$.

HOR activity measurement

Prior to electrocatalytic property testing, the Hg/HgO reference electrode was calibrated in standard three electrode system with Pt wire as working and counter electrode, and Hg/HgO electrode as the reference electrode. The 0.1 M KOH solution was purged with UHP H_2 for 30 min to obtain H_2-saturated electrolyte, and the linear sweep voltammetry (LSV) test was conducted at a scan rate of 0.5 mV/s from -0.95 V to -0.85 V vs. Hg/HgO, where the current crossed zero is taken to be the thermodynamic potential for the hydrogen electrode reactions. All reported potential in this paper was versus the reversible hydrogen electrode (RHE), which was converted by using equation of $E_{(RHE)} = E_{(Hg/HgO)} + 0.918\ V$ in 0.1 M KOH electrolyte. All applied potentials in this paper were reported versus the reversible hydrogen electrode (RHE).

The electrochemical impedance spectroscopy (EIS) measurements were performed by applying an AC voltage with 5 mV amplitude in a frequency range from 300 KHz to 100 mHz and recorded at open circuit voltage (OCV) to compensate and correct the practical potential applied on the working electrode by using following equation:

$$E_{iR-free} = E_{applied} - iR$$

where $E_{applied}$ is the applied potential on working electrode, i is corresponding measured current, R is internal resistance determined by EIS, and $E_{iR\text{-}free}$ is the internal-resistance free potential. The internal resistance of three-electrode system was measured to be ~40 Ohm in 0.1 M KOH solution.

All HOR activity measurements were carried out at room temperature. The 0.1 KOH alkaline electrolyte was purged with UHP H_2 gas at least 30 min prior to test to obtain H_2-saturated 0.1 M KOH solution. It is important to noted that H_2 could be absorbed into Pd lattice, thereby showing an extra HOR peak in its corresponding polarization curve. Thus, we have to use low scan rate to reveal the intrinsic activity of Pd-based catalysts toward HOR.

With iR-correction, the kinetic current of the HER/HOR, i_k, was calculated based on the Koutecky-Levich equation.

$$\frac{1}{i} = \frac{1}{i_k} + \frac{1}{i_d}$$

Where i is the measured current, and i_d is the limiting current. The i_k was then normalized by the geometric surface area of RDE disk (0.19625cm^2) to obtain kinetic current density, J_k.

The mass activity (MA) was normalized by using the mass of active metal drop-casted on RDE surface. For alloyed PdCu/C catalysts, only Pd was considered as active metal, whereas Cu is inert toward HOR.

$$MA = i_k / M_{active\ metal}$$

where $M_{active\ metal}$ is the mass of active metal

The specific activity (SA) was normalized by using the ECSA of active metal drop-casted on RDE surface. For alloyed PdCu/C catalysts, only Pd was considered as active metal, whereas Cu is inert toward HOR.

$$SA = i_k / ECSA_{active\ metal}$$

where $ECSA_{active\ metal}$ is the electrochemical surface area of active metal

The exchange current (i_0), and mass and specific exchange current densities ($i_{0,m}$ and $i_{0,s}$) of Pd/C, Pt/C, PdCu/C-200°C and PdCu/C-500°C were calculated by using following equations.

$$\frac{1}{i} = \frac{1}{i_k} + \frac{1}{i_d}$$

$$i_k = i_o \frac{F\eta}{RT}$$

The i_0 can be obtained by fitting the kinetic currents into the linearized Butler-Volmer equation with the assumption that the anodic and cathodic transfer coefficient summation equals to 1 ($\alpha_a + \alpha_c = 1$), and the results are shown in **Table S4**.[6]

Electrochemical surface area (ECSA) measurement by CO-stripping method

The electrochemical surface area (ECSA) of Pd in PdCu/C was determined by using CO-stripping voltammograms. The PdCu/C electrode was first stabilized through cyclic voltammetry (CV) scanning at a scan rate of 100 mV/s for at least 50 cycles under UHP N_2 purging. Afterwards, UHP CO was purged for 20 min to obtained CO-saturated solution. The electrode was subsequently held at 0.2 V vs. RHE for 15 min in CO-saturated solution, followed by another 15 min with UHP N_2 purging. The CV was then conducted between 0.2 V to 1.25 V vs. RHE with a 20 mV/s scan rate. With the positively scanning, the adsorbed CO can be oxidized, and the corresponding CO oxidation peak can be observed from the 1st cycle of CO-stripping voltammograms. After 1 cycle scanning, the adsorbed CO should be completely removed, and the total charge difference between the 1st and 2nd cycles (total charge of adsorbed CO oxidation) can be used for active metal ECSA determination by using following equation.

$$ECSA_{active\ metal} = \frac{Q}{420 \mu C\ cm^{-2} \times m}$$

where Q is the total charge of adsorbed CO oxidation, m is the total loading of active metal (e.g. Pt, or Pd), and the 420 μC cm^{-2} corresponds to a monolayer of adsorbed CO. As shown in **Figure S13b**, Cu shows no peak associated with CO oxidation, and the sharp peak at 0.85V observed from the 2nd cycle should be assigned to the further oxidation of Cu^0/Cu^{1+} to Cu^{2+}. Therefore, we hypothesize that the CO can only adsorb on Pt and Pd surface under 0.2V applied potential, and the measured charge of CO oxidation can be directly used for Pt and Pd ECSA determination. The CO-stripping voltammograms and calculated ECSA are shown in **Figure S13a** and **Table S1**.

Durability test of PdCu/C-500°C.

The durability, another important criteria used to evaluate the catalysts, was also studied, which is rarely reported in previous HOR publications. In this work, the PdCu/C-500°C were spray-coated on the acid-treated carbon cloth to simulate the practical HOR electrode in AEMFCs, and the Pt/C electrode as control group was also investigated by using the same active metal loading to PdCu/C electrode. As shown in **Figure S3a**, the measured current of PdCu/C-500°C catalyst was slight decreased, and retained about 88.0% performance compared to the initial current after 12 h. However, the Pt/C electrode shows a rapid activity drop, and only remained 70.5% of initial performance after 12h. The activity degradation of the nano-scaled catalysts in long-term durability test could be attributed to three possible reasons: 1) metal leaching out; 2) particle agglomeration; and 3) crystalline structure change. To rule out the possible reason of particle agglomeration and structure change, we compare the XRD and TEM results before and after 12h durability test. As shown in **Figure S3b**, the XRD pattern of PdCu/C electrode has no change after 12 h test, where the bcc diffraction peaks were well maintained, suggesting a good stability of bcc structure of PdCu NPs under applied potential in the absence of phase transformation. The sharp peaks centered at 44.2°, 64.5°, and 81.9° should be assigned to AS-4 polymer reflections, which can be observed from XRD patterns of blank AS-4 sprayed electrode. The TEM images (**Figure S3c**) show the similar particle size before and after 12h chronoamperometry tests, indicating rare particle agglomeration. Therefore, the performance drop could ascribe to leach-out of the Pd-Cu metal ions as evidenced by ICP-OES results that small amount of Pd and Cu were detected in the electrolyte after durability test.

III. Reference intensity ratio (RIR) method of quantitative analysis (Hillier, 2000, Clay Minerals)

The RIR method was used to estimate the fcc and bcc phase ratio in PdCu NPs from ex-situ XRD patterns. Since we only have two difference crystalline structure (defined as α and β), the RIR equation can be simplified as following:

$$X_\alpha = \frac{I_\alpha}{I_\alpha + I_\beta / K_\alpha^\beta} \text{ and } X_\beta = \frac{I_\beta}{I_\beta + I_\alpha / K_\alpha^\beta}$$

$$K_\alpha^\beta = \frac{K_{Al2O3}^\beta}{K_{Al2O3}^\alpha} = \frac{(I / I_c)_\beta}{(I / I_c)_\alpha}$$

$$(I / I_c)_{fcc} = 12.62 \text{ ; } (I / I_c)_{bcc} = 16.94$$

where X_i is the weight fraction of phase i (fcc or bcc phase); I_i is the intensity of reflection of specific facet which is defined as I=100%; K is calculated by using above equation. I/Ic is the defined as the reference intensity ratio (RIR) for a 50:50 mixture of phase α and corundum (Al_2O_3), which is so called "RIR" value. In this work, we choose the FCC-PdCu (Fm-3m(225)) ICDD 00-048-1551 and BCC-PdCu (Pm-3m(221)) ICDD 04-015-2413 standard XRD card for RIR quantitative analysis, and fcc(111) as well as bcc(110) diffraction peaks were defined as I=100% line for fcc and bcc phase, respectively. The fcc/bcc phase ratio was estimated as shown in **Figure S7**. It should be noted that the RIR quantitative analysis with corresponding peak fitting in this work is based on the standard XRD patterns of FCC-PdCu (ICDD 00-048-1551) and CsCl-structure typed BCC-PdCu (ICDD 04-015-2413) reported by previous work, and the lattice constant change of PdCu caused by thermal annealing and the 2θ angle deviation between as-synthesized PdCu and standard PdCu were not taken into consideration.

IV. Density functional theory (DFT) calculation

Density functional theory (DFT) calculations were used to investigate the adsorption and reaction energetics of *H, *OH and *H_2O on Pt, Pd and PdCu surfaces. These calculations were performed using the projected augmented wave (PAW) method[7, 8] as implemented in the Vienna *Ab* initio simulation package (VASP) 5.4.4.[9] The electron interactions were described using the Perdew–Burke–Ernzerhof (PBE) exchange-correlation functional within the generalized gradient approximation (GGA) scheme.[10] The kinetic cutoff energy for the plane-wave basis set was 700 eV. For geometric optimizations, the smearing method of Methfessel-Paxton (MP) and smearing widths of 0.2 eV were applied to all of the abovementioned metallic systems.[11]

To construct the surface slabs required to model *H, *OH and H_2O adsorption, we first optimize the lattice constants of the corresponding bulk phases. For fcc-Pt unit cell with 4 Pt atoms, our test indicated that a 24 × 24 × 24 Monkhorst–Pack k-point mesh led to an energy difference less than 0.001 eV/atom.[12] The 24 × 24 × 24 Monkhorst–Pack k-point mesh was also applied to fcc-Pd and bcc-PdCu (B2) unit cells. For fcc-PdCu bulk phase, previous studies proposed two kinds of ordered structures, namely, $L1_0$ and B13.[13] Due to their different unit cell size, we applied 13 × 13 × 13 and 6 × 6 × 6 Monkhorst–Pack k-point mesh to achieve a similar computational accuracy. All bulk phases were optimized until the magnitude of the residual forces on the atoms was less than 0.001 eV $Å^{-1}$.

For *H adsorption, to investigate the coverage effect on the adsorption energy, 1 × 1, 2 × 1 and 3 × 1 rectangular unit cells was used for PdCu-B2(110), PdCu-$L1_0$(111) and PdCu-B13(111). The *H coverage was thus 1/2 ML, 1/4 ML and 1/6 ML, respectively. The same coverage was achieved on Pt(111) and Pd(111) using 1 × 2, 2 × 2 and 3 × 2 rectangular unit cells. 24 × 18 × 1, 12 × 18 × 1 and 8 × 18 × 1 Monkhorst–Pack k-point meshes were used to sample the corresponding reciprocal spaces. For *OH and *H_2O adsorption, a 3 × 1 rectangular unit cell for PdCu-B2(110), PdCu-$L1_0$(111) and PdCu-B13(111) and a 3 × 2 rectangular unit cell for Pt(111) and Pd(111) were found to be the smallest periodic unit that can repeat the hexagonal ice like water structure. 1/3 ML *OH and 1/3 ML *H_2O arrangement was achieved for *OH adsorption. All surface calculations used 4-layer slabs with the bottom two layers fixed to their bulk position, and the vacuum spaces between periodic images were set no less than 14 Å. The Pd enrichment in PdCu alloys observed by experiment was modelled by constructing a full Pd outermost layer. The structural optimization was regarded as complete when the magnitude of the forces on the atoms was less than 0.01 eV $Å^{-1}$. Dipole corrections were included in all surface calculations in the surface normal direction for both energies and forces. The frequencies of the surface adsorbed species were computed using finite difference method, and zero-point energy as well as vibrational entropy was computed with standard methods and harmonic oscillator approximation to convert electronic DFT energy into free energy.[14] The entropy term of free molecular species was referred to JANAF thermodynamic table.[15] All DFT calculations were spin-unpolarized. Coordinates of the optimized structures are available in the supporting information.

Calculating *H and *OH Equilibrium Adsorption Potential

Theoretically, the procedure of adsorption potential calculation for certain cations and anions has been well established.[16] The reductive hydrogen adsorption is shown in Equation (1):

$$*+\mathrm{H}^{+}+e^{-}\rightarrow *\mathrm{H} \quad (1)$$

The free energy change for hydrogen adsorption can be written as Equation (2):

$$\Delta G_{*\mathrm{H}}=G_{*\mathrm{H}}-G_{*}-G_{\mathrm{H}^{+}}+|e|(U-U_{\mathrm{RHE}})+\frac{\mu_{*\mathrm{H}}-\mu_{*}}{d}|e|(U-U_{\mathrm{RHE}}) \quad (2)$$

Note that we include the dipole correction before and after *H formation in the last term in Equation (2), where *d* denotes Helmholtz layer thickness, taken as 3 Å. Therefore, the equilibrium adsorption potential vs. RHE scale can be written as Equation (3):

$$U_{*\mathrm{H}}^{\mathrm{O}}=-\frac{G_{*\mathrm{H}}-G_{*}-\frac{1}{2}G_{\mathrm{H}_2}}{|e|(1+\frac{\mu_{*\mathrm{H}}-\mu_{*}}{d})} \quad (3)$$

In the above equation, the energy relation between the chemical potential of proton in RHE and gaseous H_2 in standard state is established using computational hydrogen electrode (CHE) model.[17]

Similarly, the oxidative adsorption of hydroxyl anion (OH^-) can be described as shown in Equation (4):

$$*+OH^- - e^- \rightarrow *OH \quad (4)$$

Using thermodynamic equivalent principle, Equation (4) can be rewritten as Equation (5):

$$* + H_2O_{(aq)} - e^- \rightarrow *OH + H^+_{(aq)} \quad (5)$$

After further considering the weakly adsorbed water structure and water-solvated *OH structure, the above equation can be written as Equation (6):

$$4 * H_2O - 2e^- \rightarrow 2 * OH * H_2O + 2H^+_{(aq)} \quad (6)$$

Applying the CHE model and dipole correction again, we arrive to Equation (7) for hydroxyl equilibrium potential vs. RHE scale:

$$U^{O}_{*OH} = \frac{G_{*2OH*2H_2O} - G_{*4H_2O} + G_{H_2}}{2|e|(1 + \frac{\mu_{*2OH*2H_2O} - \mu_{*4H_2O}}{d})} \quad (7)$$

Volcano Plot Construction

The adsorption potential of H and OH data (U_{ad}(H) and U_{ad}(OH)) and the exchange current densities on various metal surfaces were adopted from the previous sections "Calculating *H and *OH Equilibrium Adsorption Potential" and "The exchange current (i_0), and mass and specific exchange current densities ($i_{0,m}$ and $i_{0,s}$)" in supporting information. We furthermore integrated the previous published specific exchange current density data by Yan's group into our data to extend the range of metals investigated.[18]. We first plotted two volcano plots of $i_{0,s}$ with respect to U_{ad}(H) or U_{ad}(OH) (denoted as two-parameter volcano plots), respectively, and we found that they conform to different peak positions and different slopes of the binding legs, suggesting that the correlation between H and OH adsorption is poor, and that H and OH adsorption could be regarded as two independent parameters which determined the exchange current densities. The three-parameter volcano plot shown in **Figure 10** was therefore generated by taking square root of the multiplied exponential fitting function in $i_{0,s}$- U_{ad}(H) and $i_{0,s}$-U_{ad}(OH).

The 1/6 ML coverage H and 1/3 ML coverage OH adsorption potential (denoted as U_{ad}(H) and U_{ad}(OH)) on these PdCu close packed surfaces as well as those on Pt(111), Pd(111), Cu(111), Ni (111), Co (111), Ag (111), and W (110), were calculated and employed for volcano plot fitting in **Figure 10**.

V. Supporting Figures

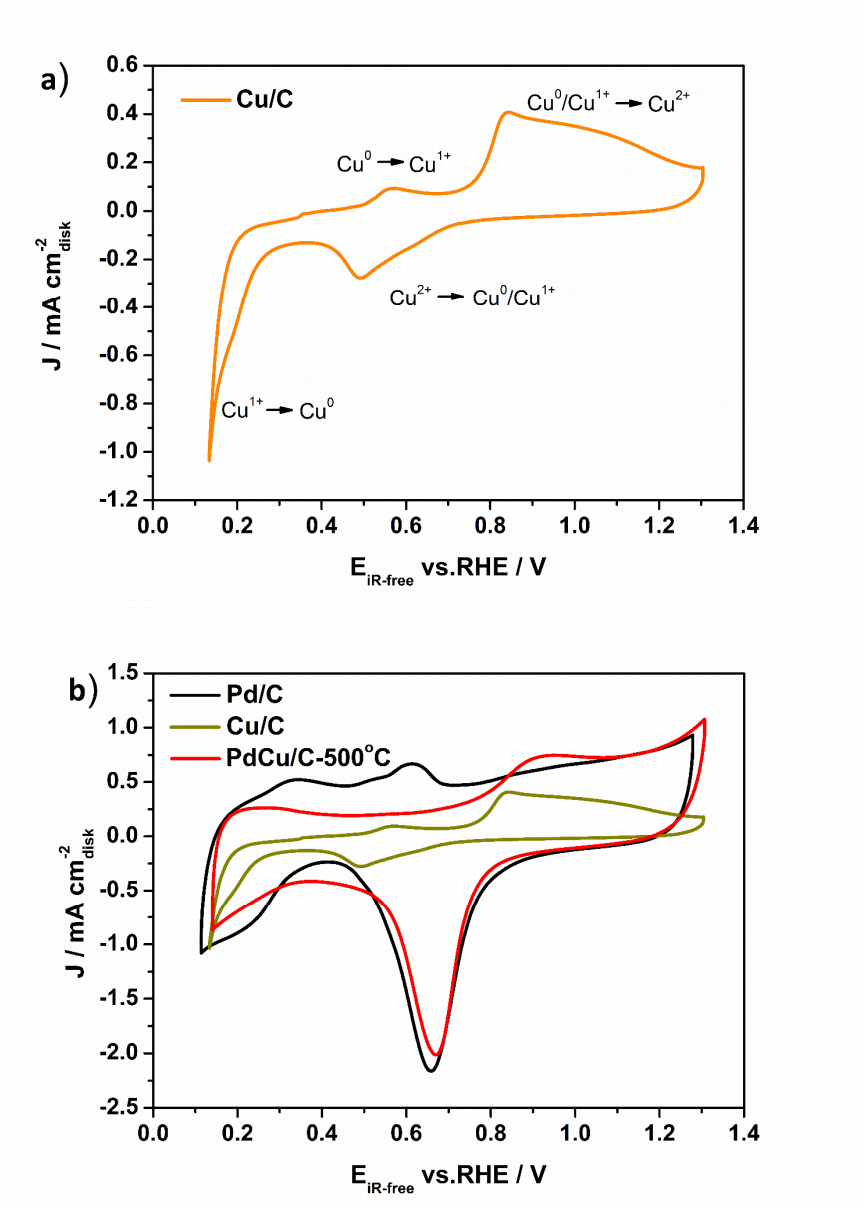

Figure S1. Cyclic voltammograms of Pd/C, Cu/C, and PdCu/C-500°C at a scan rate of 50 mV s^{-1}, 0.1 M KOH, room temperature.

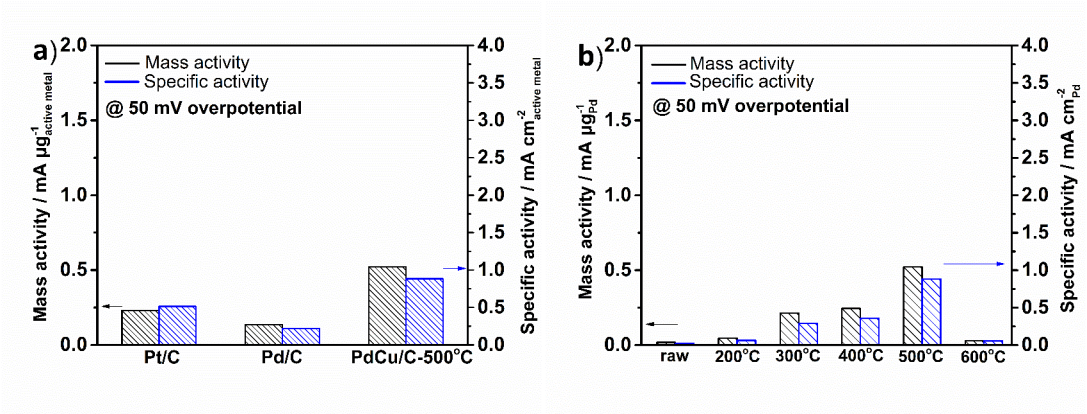

Figure S2. Comparison of HOR mass and specific activity (MA and SA) of Pt/C, Pd/C, and PdCu/C at 50mV overpotential in H_2-saturated 0.1 M KOH electrolyte.

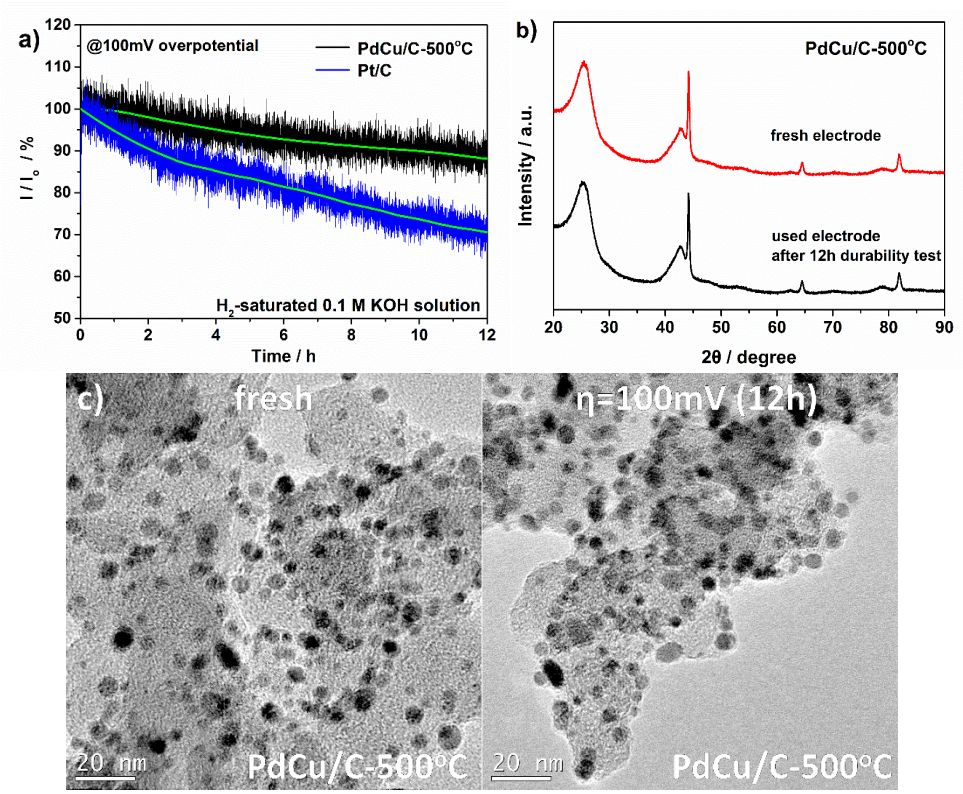

Figure S3. a) Plot of current ratio, I/I_o, as a function of time for PdCu/C-500°C at 1600rpm in H_2-saturated 0.1 M KOH solution; b) XRD patterns and c) TEM images of PdCu/C-500°C before and after 12h durability test (Detail of durability test, see "Durability test of PdCu/C-500°C" section in Supporting information).

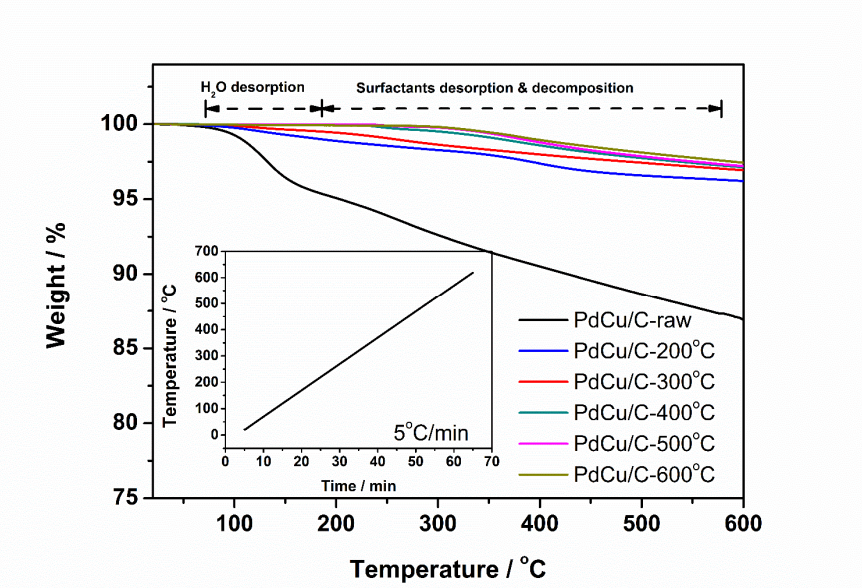

Figure S4. TGA results of PdCu-based materials under UHP N_2 conditions.

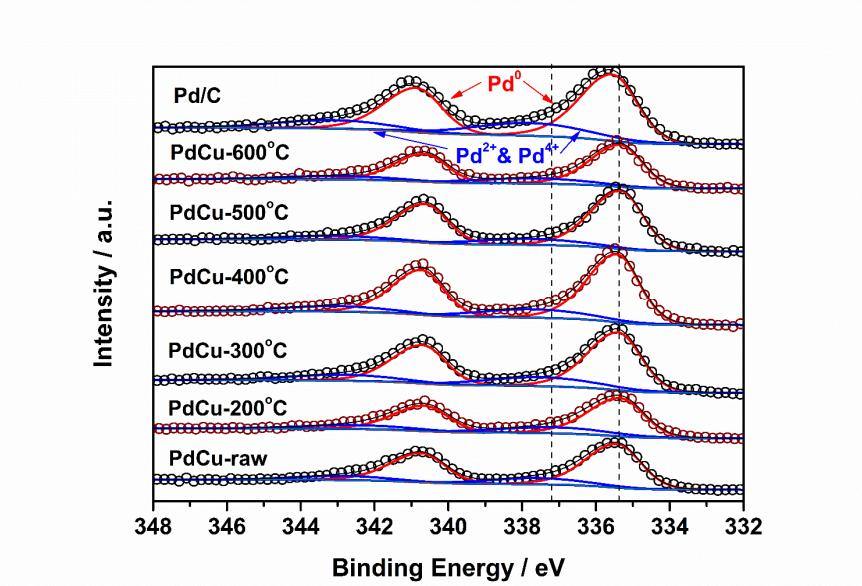

Figure S5. XPS high-resolution spectra of Pd 3d narrow scan of Pd/C and PdCu/C catalysts.

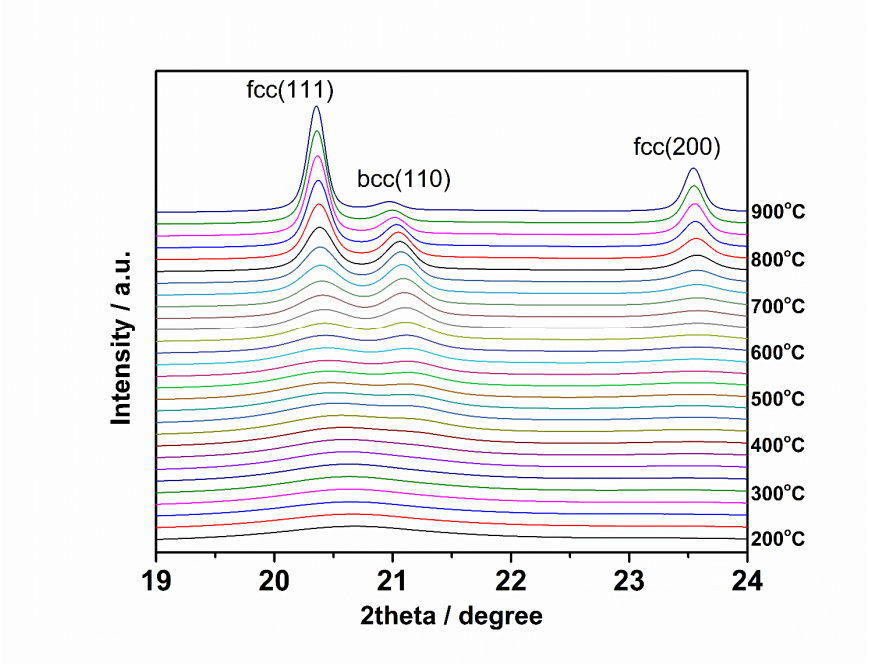

Figure S6 Selected HE-XRD patterns of PdCu/C-raw under the protocol of ramped annealing from 200°C to 900°C at 2°C min^{-1} heating rate in UHP N_2 gas flow.

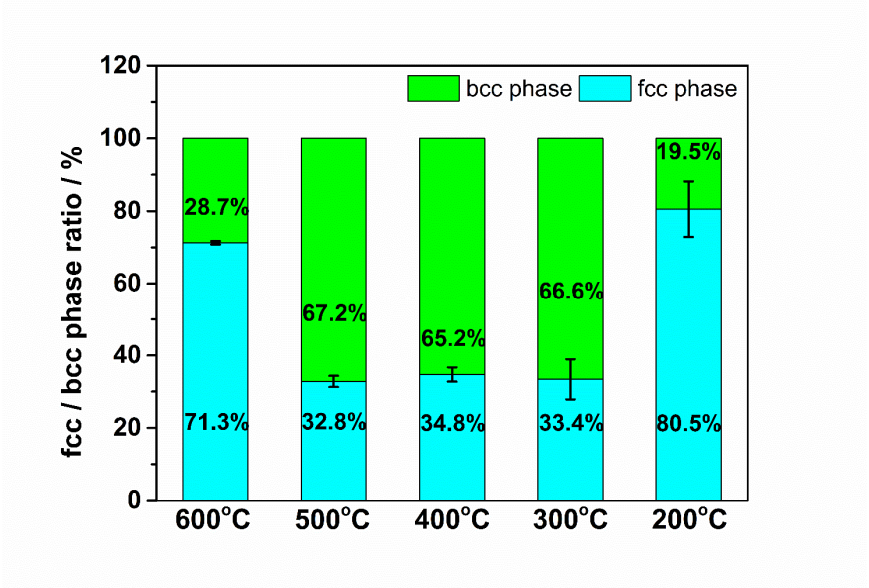

Figure S7 XRD RIR quantitative analysis of FCC / BCC ratio of PdCu/C-T (T=200 °C to 600 °C) by using ex-situ XRD patterns.

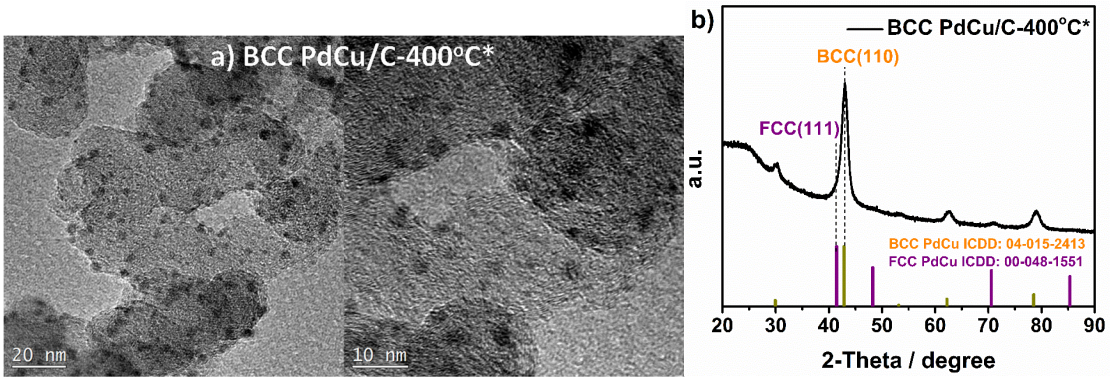

Figure S8 a) TEM images and b) XRD pattern of BCC PdCu/C-400°C*.

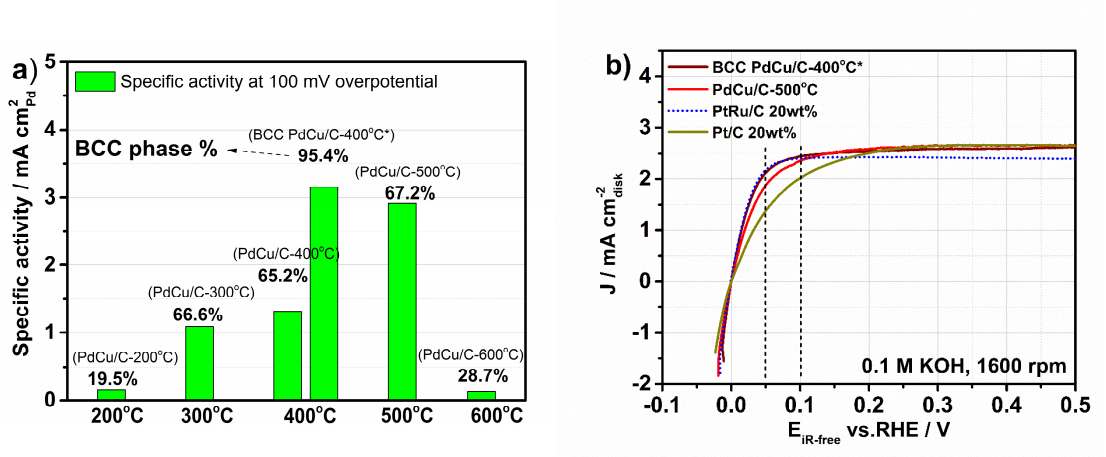

Figure S9 a) HOR specific activity dependence of BCC phase concentration over PdCu/C catalysts. b) HOR/HER polarization curves (forward scan) of BCC PdCu/C-400°C*, PdCu/C-500°C, commercial PtRu/C 20wt%, and Pt/C 20wt% samples

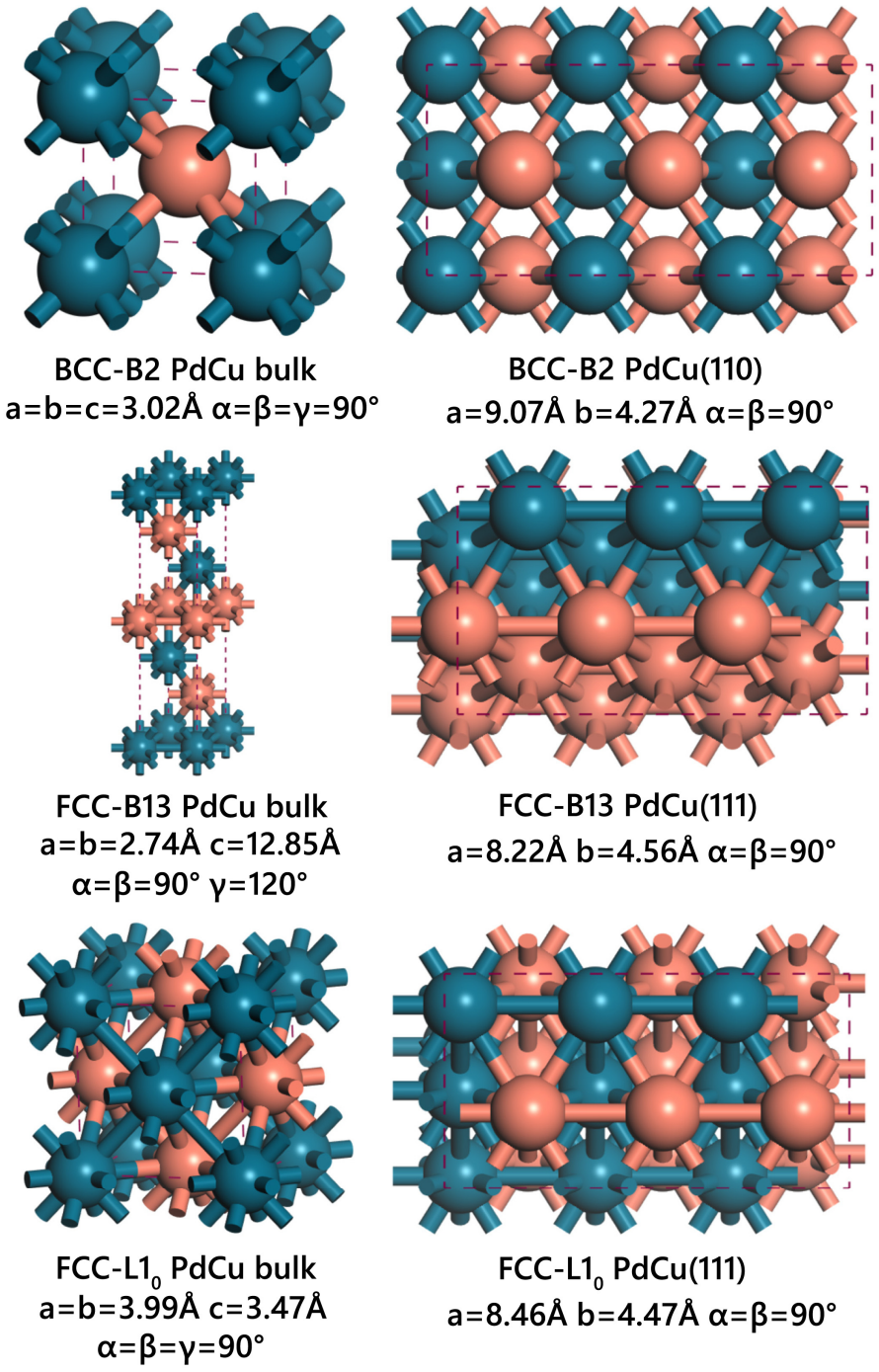

Figure S10. Structures and lattice parameters of BCC and FCC PdCu bulk and close packed surface.

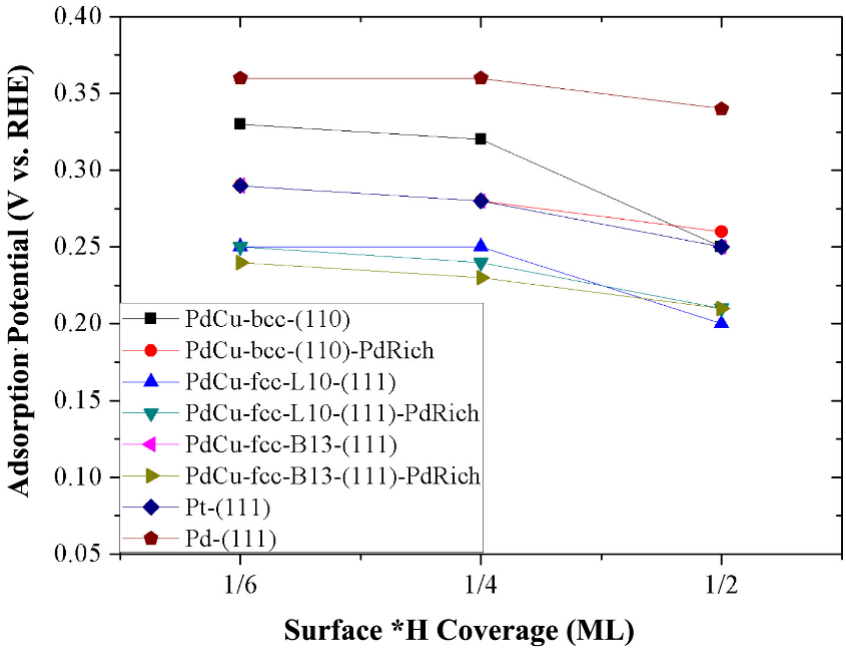

Figure S11. *H equilibrium adsorption potential with respect to surface coverage on different surfaces. The variation is generally small from 1/6 ML to 1/2 ML, and surface Pd enrichment leads to variation of *H adsorption potential within 0.05 V on bcc- and fcc-PdCu surfaces.

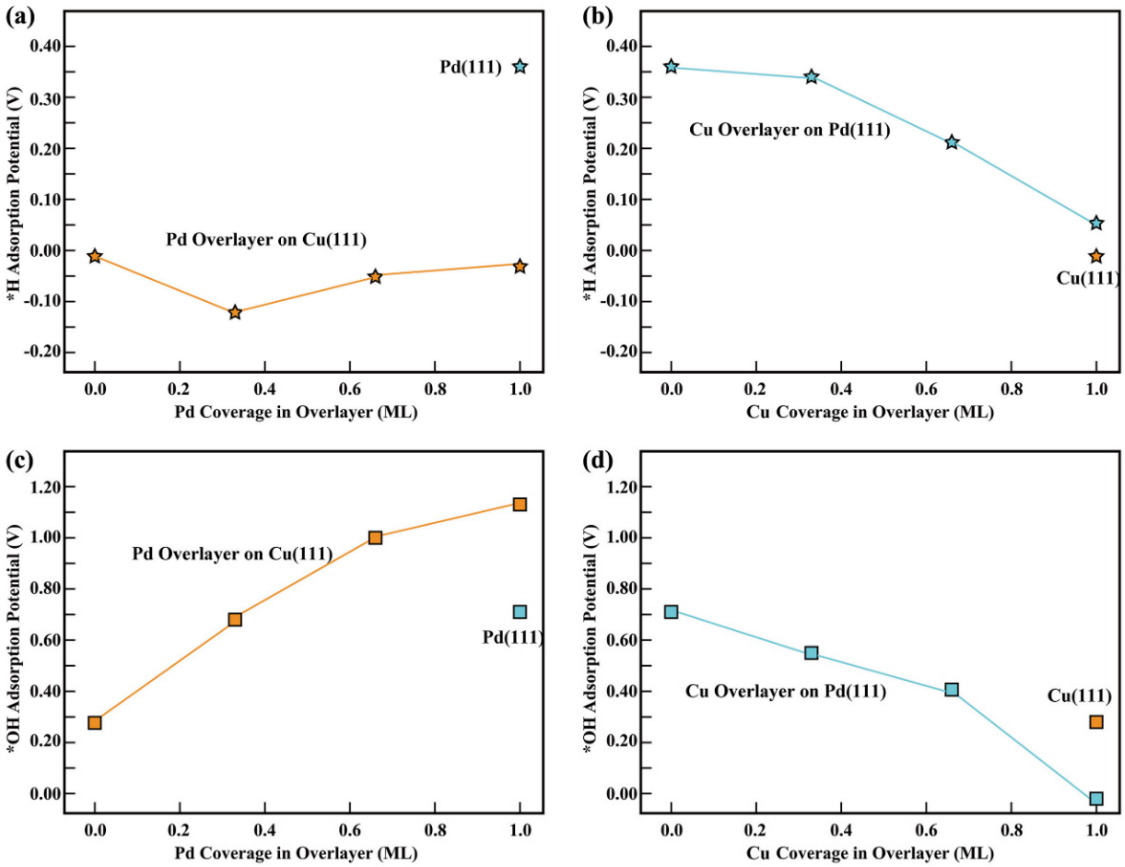

Figure S12. Equilibrium adsorption potentials (VRHE) for *H on (a) PdCu overlayer on Cu(111) and (b) PdCu overlayer on Pd(111); Equilibrium adsorption potentials (VRHE) for *OH on (c) PdCu overlayer on Cu(111) and (d) PdCu overlayer on Pd(111).

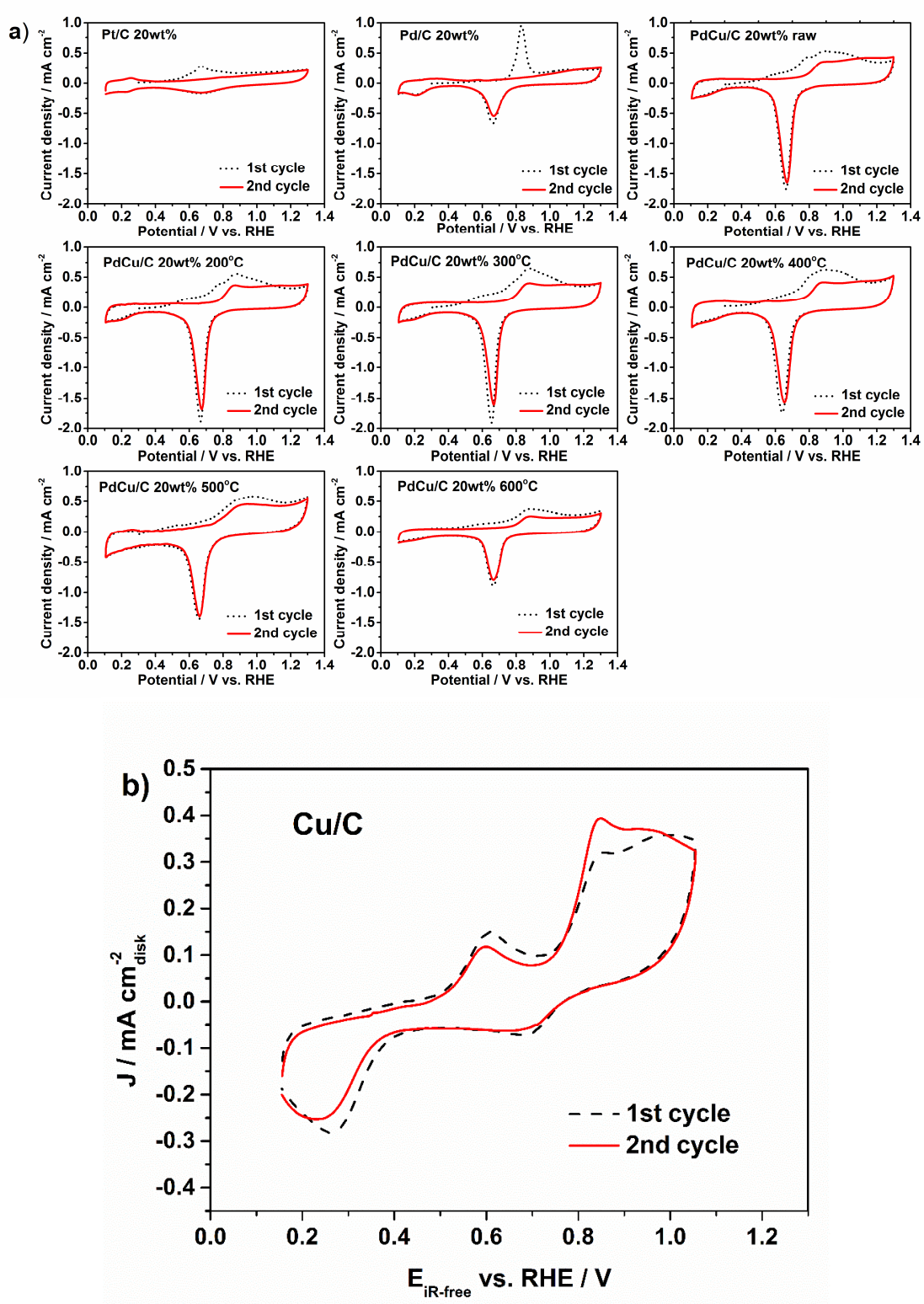

Figure S13 CO-stripping voltammograms of a) Pt/C, Pd/C, PdCu/C materials, and b) Cu/C.

VI. Supporting Tables

Table S1. Summary of half wave potential, ECSA, MA and SA as 50 mV and 100 mV overpotential of different catalysts in this work

	$E_{1/2}$	ECSA	@ 50mV over-potential			@ 100mV over-potential		
			J_k	MA	SA	J_k	MA	SA
Pt/C	0.047 V	44.6 m^2/g	2.870 mA/cm^2_{disk}	0.229 $mA/\mu g_{pt}$	0.514 mA/cm^2_{Pt}	8.504 mA/cm^2_{disk}	0.680 $mA/\mu g_{Pt}$	1.525 mA/cm^2_{Pt}
Pd/C	0.069 V	61.9 m^2/g	1.695 mA/cm^2_{disk}	0.135 $mA/\mu g_{Pd}$	0.219 mA/cm^2_{Pd}	4.820 mA/cm^2_{disk}	0.385 $mA/\mu g_{Pd}$	0.623 mA/cm^2_{Pd}
Cu/C	N/A	N/A		N/A			N/A	N/A
PdCu/C-raw	0.204 V	73.5 m^2/g	0.224 mA/cm^2_{disk}	0.018 $mA/\mu g_{Pd}$	0.024 mA/cm^2_{Pd}	0.627 mA/cm^2_{disk}	0.050 $mA/\mu g_{Pd}$	0.068 mA/cm^2_{Pd}
PdCu/C-200°C	0.145 V	72.3 m^2/g	0.572 mA/cm^2_{disk}	0.046 $mA/\mu g_{Pd}$	0.063 mA/cm^2_{Pd}	1.395 mA/cm^2_{disk}	0.112 $mA/\mu g_{Pd}$	0.152 mA/cm^2_{Pd}
PdCu/C-300°C	0.050 V	73.8 m^2/g	2.660 mA/cm^2_{disk}	0.213 $mA/\mu g_{Pd}$	0.288 mA/cm^2_{Pd}	10.061 mA/cm^2_{disk}	0.804 $mA/\mu g_{Pd}$	1.091 mA/cm^2_{Pd}
PdCu/C-400°C	0.046 V	68.9 m^2/g	3.065 mA/cm^2_{disk}	0.245 $mA/\mu g_{Pd}$	0.356 mA/cm^2_{Pd}	11.323 mA/cm^2_{disk}	0.906 $mA/\mu g_{Pd}$	1.315 mA/cm^2_{Pd}
PdCu/C-500°C	0.028 V	59.1 m^2/g	6.528 mA/cm^2_{disk}	0.522 $mA/\mu g_{Pd}$	0.883 mA/cm^2_{Pd}	21.590 mA/cm^2_{disk}	1.727 $mA/\mu g_{Pd}$	2.922 mA/cm^2_{Pd}
PdCu/C-600°C	0.184 V	50.6 m^2/g	0.350 mA/cm^2_{disk}	0.028 $mA/\mu g_{Pd}$	0.055 mA/cm^2_{Pd}	0.818 mA/cm^2_{disk}	0.065 $mA/\mu g_{Pd}$	0.129 mA/cm^2_{Pd}
BCC PdCu/C-400°C*	0.021 V	80.6 m^2/g	11.347 mA/cm^2_{disk}	0.768 $mA/\mu g_{Pd}$	0.953 mA/cm^2_{Pd}	37.450 mA/cm^2_{disk}	2.534 $mA/\mu g_{Pd}$	3.145 mA/cm^2_{Pd}

Table S2. Literature summary of HOR catalysts

	Electrolyte	@ 50mV over-potential		@ 100mV over-potential		Ref
		MA	SA	MA	SA	
PdCu/C-300°C	0.1 M KOH	0.213 $mA/\mu g_{pd}$	0.288 mA/cm^2_{Pd}	0.804 $mA/\mu g_{Pd}$	1.091 mA/cm^2_{Pd}	This work
PdCu/C-400°C	0.1 M KOH	0.245 $mA/\mu g_{pd}$	0.356 mA/cm^2_{Pd}	0.906 $mA/\mu g_{Pd}$	1.315 mA/cm^2_{Pd}	This work
PdCu/C-500°C	0.1 M KOH	**0.522 $mA/\mu g_{pd}$**	**0.883 mA/cm^2_{Pd}**	**1.727 $mA/\mu g_{Pd}$**	**2.922 mA/cm^2_{Pd}**	This work
Ni/N-CNT	0.1 M KOH	0.009 $mA/\mu g_{Ni}$	0.05 mA/cm^2_{Ni}	-	-	1
CoNiMo	0.1 M KOH	-	0.044 mA/cm^2_{Pd}		0.069 mA/cm^2_{Pd}	2
Pd/CuNW	0.1 M KOH	0.76 $mA/\mu g_{Pd}$	2.21 mA/cm^2_{Pd}	0.934 $mA/\mu g_{Pd}$	2.84 mA/cm^2_{Pd}	3
PdNT (Cu)	0.1 M KOH	0.123 $mA/\mu g_{Pd}$	2.01 mA/cm^2_{Pd}	0.137 $mA/\mu g_{Pd}$	2.43 mA/cm^2_{Pd}	3
PtRu NWs	0.1 M KOH	0.6 $mA/\mu g_{Pt}$	-	1.667 $mA/\mu g_{Pt}$	-	4
PtCo NWs	0.1 M KOH	0.307 $mA/\mu g_{Pt}$	-	0.850 $mA/\mu g_{Pt}$	-	4
PtRu/C	0.1 M KOH	1.023 $mA/\mu g_{Pt}$	1.463 mA/cm^2_{Pt}	2.307 $mA/\mu g_{Pt}$	3.286 mA/cm^2_{Pt}	This work

*commercial PtRu/C 20wt% was investigated in this work as control sample

Table S3. Summary Pd/Cu ratio of PdCu catalysts determined by ICP-OES

	Pd / at.%	Cu / at.%
PdCu/C-raw	56.80%	43.20%
PdCu/C-200°C	56.50%	43.50%
PdCu/C-300°C	56.74%	43.26%
PdCu/C-400°C	55.64%	44.36%
PdCu/C-500°C	55.97%	44.03%
PdCu/C-600°C	55.81%	44.19%

Table S4. Summary of mass and specific activity current densities determined from linearized Butler-Volmer equation with the assumption that $\alpha_a + \alpha_c = 1$ in 0.1 M KOH

	i_o	$i_{o,m}$	$i_{o,s}$	$\log_{10}(i_{o,s}$ (A/cm^2))
PdCu/C-200°C	0.0282 mA	11.2892 mA/mg$_{Pd}$	0.0156 mA/cm$^2_{Pd}$	-4.8
PdCu/C 500°C	0.3190 mA	127.6172 mA/mg$_{Pd}$	0.2159 mA/cm$^2_{Pd}$	-3.6
Pd/C	0.0939 mA	37.5692 mA/mg$_{Pd}$	0.0607 mA/cm$^2_{Pd}$	-4.2
Pt/C	0.2054 mA	82.1678 mA/mg$_{Pt}$	0.1842 mA/cm$^2_{Pt}$	-3.7
*Polycrystalline Ag	-	-	0.000050 mA/cm$^2_{Ag}$	-7.3
*Polycrystalline Cu	-	-	0.00158 mA/cm$^2_{Cu}$	-5.8
*Polycrystalline Pt	-	-	0.6309 mA/cm$^2_{Pt}$	-3.2
*Polycrystalline Pd	-	-	0.1259 mA/cm$^2_{Pd}$	-3.9
*Polycrystalline Co	-	-	0.00316 mA/cm$^2_{Co}$	-5.5
*Polycrystalline Ni	-	-	0.00794 mA/cm$^2_{Ni}$	-5.1
*Polycrystalline W	-	-	0.000063 mA/cm$^2_{W}$	-7.2

* $i_{o,s}$ is determined by using polycrystalline metal disk electrode.[18]

VII. References

(1) Zhuang, Z. B.; Giles, S. A.; Zheng, J.; Jenness, G. R.; Caratzoulas, S.; Vlachos, D. G.; Yan, Y. S. *Nat. Commun.* **2016**, *7*, 10141.

(2) Sheng, W. C.; Bivens, A. P.; Myint, M.; Zhuang, Z. B.; Forest, R. V.; Fang, Q. R.; Chen, J. G.; Yan, Y. S. *Energy Environ. Sci.* **2014**, *7*, 1719.

(3) Alia, S. M.; Yan, Y. S. *J. Electrochem. Soc.* **2015**, *162*. F849

(4) Scofield, M. E.; Zhou, Y. C.; Yue, S. Y.; Wang, L.; Su, D.; Tong, X.; Vukmirovic, M. B.; Adzic, R. R.; Wong, S. S. *ACS Catal.* **2016**, *6*, 3895.

(5) Qiu, Y.; Xin, L.; Li, W. Z. *Langmuir* **2014**, *30*, 7893.

(6) Zheng, J.; Zhou, S. Y.; Gu, S.; Xu, B. J.; Yan, Y. S. *J. Electrochem. Soc.* **2016**, *163*, F499.

(7) Blöchl, P. E. *Phys. Rev. B* **1994**, *50*, 17953.

(8) Kresse, G.; Joubert, D. *Phys. Rev. B* **1999**, *59*, 1758.

(9) Kresse, G.; Furthmüller, J. *Phys. Rev. B* **1996**, *54*, 11169.

(10) Perdew, J. P.; Burke, K.; Ernzerhof, M. *Phys. Rev. Lett.* **1996**, *77*, 3865.

(11) Methfessel, M.; Paxton, A. T. *Phys. Rev. B* **1989**, *40*, 3616.

(12) Monkhorst, H. J.; Pack, J. D. *Phys. Rev. B* **1976**, *13*, 5188.

(13) Sha, Y.; Yu, T. H.; Merinov, B. V.; Goddard, W. A. *ACS Catal.* **2014**, *4*, 1189.

(14) McQuarrie, D. A.; Simon, J. D. *Molecular Thermodynamics*; University Science Books, 1999.

(15) Stull, D. R.; Prophet, H. *JANAF thermochemical tables*, National Standard Reference Data System, 1971.

(16) McCrum, I. T.; Janik, M. J. *J. Phys. Chem. C* **2016**, *120*, 457.

(17) Nørskov, J. K.; Rossmeisl, J.; Logadottir, A.; Lindqvist, L.; Kitchin, J. R.; Bligaard, T.; Jónsson, H. *J. Phys. Chem. B* **2004**, *108*, 17886.

(18) Sheng, W.; Myint, M.; Chen, J. G.; Yan, Y. *Energy Environ. Sci.* **2013**, *6*, 1509.